Insight into the wetting of a graphene-mica slit pore with a monolayer of water

Hu Lin, Andre Schilo, A. Rauf Kamoka, Nikolai Severin, Igor M. Sokolov, and Jürgen P. Rabe
Department of Physics & IRIS Adlershof, Humboldt-Universität zu Berlin, Newtonstraße 15, 12489 Berlin, Germany
(Received 21 December 2016; revised manuscript received 24 March 2017; published 12 May 2017)

Scanning force microscopy (SFM) and Raman spectroscopy allow the unraveling of charge doping and strain effects upon wetting and dewetting of a graphene-mica slit pore with water. SFM reveals a wetting monolayer of water, slightly thinner than a single layer of graphene. The Raman spectrum of the dry pore exhibits the D' peak of graphene, which practically disappears upon wetting, and recurs when the water layer dewets the pore. Based on the $2D$- and G-peak positions, the corresponding peak intensities, and the widths, we conclude that graphene on dry mica is charge-doped and variably strained. A monolayer of water in between graphene and mica removes the doping and reduces the strain. We attribute the D' peak to direct contact of the graphene with the ionic mica surface in dry conditions, and we conclude that a complete monolayer of water wetting the slit pore decouples the graphene from the mica substrate both mechanically and electronically.

DOI: 10.1103/PhysRevB.95.195414

I. INTRODUCTION

The properties of molecularly thin films of liquids confined in nanoscopic pores are both scientifically interesting and practically important. For instance, understanding the transport of water through soft nanoscopic pores is important for the design of filtration membranes [1,2].

Graphene covering molecular films or single molecules on an atomically flat mica surface can replicate the topography of the adsorbates [3,4]. This system has been considered therefore as a model for a soft slit pore [5], which enables high-resolution imaging of its content by scanning force microscopy (SFM). Muscovite mica, a naturally occurring layered crystal, can be easily cleaved to produce atomically flat and clean hydrophilic surfaces [6]. It has been extensively used to investigate rheological properties of liquids squeezed between its surface and another solid surface [7–9]. High-resolution SFM imaging of graphene replicating the topography of thin-fluid films on a mica surface can potentially provide further insight into the properties of thin films, particularly of water films confined in this soft slit pore [10–14]. However, the properties of these water films remain controversial, not the least because of the limited information accessible so far. Particularly, it is difficult to obtain direct spectroscopic information from the ultrathin water films, since, e.g., the Raman cross section of the water is very small.

In experimental studies information on the structure of the films has been deduced from the height and lateral shape of graphene replicas of water islands. A height of 3.7 ± 0.2 Å was reported and argued to indicate the I_h ice bilayer [3]. The icelike nature of the islands was further supported by the shape persistence of the islands, implied by the correlation of surface coverage with the ambient humidity during sample preparation. It was also shown that the structure, i.e., the thickness of the water film and its properties, depends sensitively on molecular additives possibly originating from adhesive tape used to exfoliate graphenes onto a substrate [15]. An adhesive tape-free exfoliation of graphenes has been argued to provide fluid films of water since the films wetted the slit pore upon increase, and dewetted the pore upon reduction of humidity [5]. The depth of the dewetting patterns was reported to be 2.8 ± 0.5 Å, implying a monomolecular thickness of the film. However, the depth of the dewetting patterns matching I_h ice bilayer has also been reported, implying an icelike structure of the fluid layer [16,17]. Therefore, the fluidity of the film was questioned and the growth of the dewetting patterns was attributed to diffusion of water molecules along the edges of the growing patterns [16]. Furthermore, it has also been suggested that the shape-changing layer is situated on top of another homogeneous layer of water molecules, such that the total film filling the slit pore is even thicker [16]. The thicker film was used to explain the observed saturation of the dewetting.

In contrast to water, graphene exhibits strong Raman scattering [18,19]. Furthermore, Raman spectroscopy allows one to precisely quantify strain and charge-doping in single-layer graphene [20]. Therefore Raman spectroscopy may be considered as a sensitive tool for tracing molecules wetting the soft slit pore and affecting graphene charge-doping and strain. For example, graphenes were argued to be p-doped when in a direct contact with mica surface, with a single bilayer of I_h water ice confined between graphene and mica blocking the charge transfer [21].

The aim of our work was to gain further insight into the properties of a water layer wetting the slit pore. For this we exfoliated graphenes onto freshly cleaved mica under dry nitrogen, then increased the humidity and followed the wetting of the graphene-mica slit pores with water by SFM and Raman spectroscopy. We show that the thickness of the wetting layer is smaller than the height expected for a bilayer of water molecules, and that it rather matches the size of single water molecules. Furthermore, we argue that in dry pores graphene is in direct contact with mica, while a monolayer of water wetting the slit pore decouples the graphene from the mica substrate both mechanically and electronically.

II. EXPERIMENTAL SECTION

The slit pores were prepared by mechanical exfoliation of highly oriented pyrolytic graphite (HOPG, grade ZYA, Momentive Performance Inc.) onto a freshly cleaved muscovite mica surface [Ratan Mica Exports, grade V1 (optical quality)] in a glove box (LABmaster, M. Braun Inertgas-Systeme GmbH) filled with nitrogen and less than 10 ppm of

water. Thin graphite flakes were peeled off a piece of freshly cleaved HOPG and put onto the mica surface with a pair of tweezers. The tweezers were electrically grounded to remove any possible electric charges from the flakes. The flakes were removed after a few minutes with the same tweezers. Single-layer graphenes (SLGs) were detected with an optical microscope located inside the glove box [22]. The samples were then further used for either scanning force microscopy imaging or Raman investigations at variable humidities.

The scanning force microscope (Digital Instruments, Multimode, Nanoscope IV) was operated with either E- or J scanners in tapping mode at a typical rate of 3 min per image. Image height calibration was performed assuming 0.34 nm for the step height between successive graphene layers. Silicon cantilevers with typical resonance frequencies of 300 kHz and spring constants of 26 and 42 N/m (OMCL-AC160TS and OMCL-AC160TSG, respectively, Olympus Corporation) were used. The tips exhibited a typical apex radius of 7 nm as specified by the manufacturer. The SFM images were processed and analyzed with SPIP (Image Metrology A/S) image-processing software. A first- or second-order line subtraction and manual plane tilt were applied to SFM height images to compensate for drifts, image bow, and sample inclinations. Graphenes were first imaged with the SFM instrument located inside the glove box. Then, the SFM instrument was moved into a homebuilt environmental control chamber located inside the glove box. The chamber was sealed and humidity inside the chamber was raised by purging the chamber with dry nitrogen bubbling through a gas wash bottle filled with deionized and purified water (Protegra CS Systems CEDI Technology >10 MΩ cm). Relative humidity (RH) inside the chamber was measured with a Testo 625 thermo-hygrometer (Testo Inc.) equipped with a remote sensor. The RH instrument calibration fidelity is ±2.5% as specified by the manufacturer. Provided RH values are the displayed ones. Nitrogen (Linde group) had 99.999% purity as specified by the manufacturer, with both water and oxygen content less than 2 ppm. A combination of stainless steel and polytetrafluoroethylene and/or fluorinated ethylene propylene (Carl Roth GmbH) pipes was used to route nitrogen.

Raman measurements were performed with a confocal Raman microscope (XploRA, Horiba Ltd.) with 2400 lines/mm grating and spectral resolution better than 1.4 cm^{-1}. The excitation laser was 532 nm with 1.4 mW illumination intensity on the sample surface. The Raman spectroscope was calibrated before and after each day of experiment, using benzonitrile (Sigma-Aldrich, Chromasolv 99.9%) and cyclohexane (Sigma-Aldrich, Chromasolv Plus >99.9%) according to ASTM E1840 standard. Standard peak positions of benzonitrile (1598.9 ± 0.7 cm^{-1}) and cyclohexanes (2664.4 ± 0.4 cm^{-1}) were used to correct graphene G and $2D$ peak positions, respectively. Calibration drift, i.e., the shift of the aforementioned peak positions, did not exceed 1 cm^{-1} over a day of measurements. The error of the peak position was calculated as the sum of the ASTM E1840 errors specified above and half of the calibration drift. Mica with graphenes exfoliated thereon was fixed onto a homebuilt gas cell with graphenes facing the inner cell chamber and mica acting as a semitransparent lid. Mica was mounted onto the gas cell inside the glove box. The gas cell was then additionally sealed inside a plastic box and transferred to the Raman instrument. The sealing was removed and the cell was subjected to a continuous nitrogen flow within a few seconds after removal of the sealing. The nitrogen flow was passing through a 31 × 31 × 40 cm large acryl box connected before the gas cell with the RH sensor located inside. The RH values provided are the readout values. RH of the nitrogen gas was controlled by mixing dry nitrogen with nitrogen bubbling through a gas washing bottle filled with deionized and purified water (Protegra CS Systems CEDI Technology >10 MΩ cm). The delay between the onset of humid nitrogen flow and Raman measurements was at least 1 h. For the test of the D' reactivation, RH was increased to 50% by bubbling the nitrogen flow through the gas washing bottle filled with water and then the flow was stopped when the desired RH value was reached. The cell was dried with a continuous flow of nitrogen.

The microscope objective was manually focused onto a piece of single-layer graphene. Then, an overview spectrum in the range from 1200 to 2800 cm^{-1} and with 30 s accumulation time was acquired. The overview spectra were used to calculate the $2D$ to G peak area ratios in order to minimize the influence of possible focal drifts. Then, a high-resolution spectrum in the range 1200 to 1800 cm^{-1} and with 300 s accumulation time was acquired and used to estimate the D and D' peaks. The spectra were processed with the LAB SPEC 6 (Horiba) software. Peaks in the spectra were fitted with Lorentz functions in ORIGINPRO 8.6 (OriginLab Corporation). The peak areas, positions, and full width at half maximum (FWHM) values provided are the values of the fits.

III. RESULTS

Single- and few-layer graphenes on mica were atomically flat, provided they were both exfoliated and imaged in dry nitrogen with less than 10 ppm of water. Upon increasing the relative humidity to about 10%, elevated flat islands appeared on graphene-covered areas at the graphene-mica edges. They grew laterally both with time and increasing humidity, propagating from the edges into graphene-covered areas [Figs. 1(a) and 1(b)]. Phase images, which map the phase lag between driving force and cantilever oscillations, showed a strong contrast between graphene-covered and -uncovered mica, but rather weak or no contrast between the islands and the surrounding graphene. We tentatively attribute the islands to a layer of water molecules moving into the slit pore from its free edges, and will discuss this in more detail below. The water islands grew together as the humidity increased further, eventually leading again to perfectly flat graphenes at around 50% RH. The step height of the islands was 2.8 ± 0.5 Å, with the error here and in the following being the standard deviation unless noted otherwise.

Since the upper bound on the height of the water layer will be crucial in the following arguments, we looked for additional means to determine it. For this purpose, we searched multilayer graphene areas for single-layer graphene steps with the lower terrace filled and upper terrace yet not filled with a water layer [Fig. 1(c)]. The surface of a slit pore with n layers of graphene filled with water was lower than the surface of the neighboring slit pore with $(n + 1)$ layers of graphene and not filled with water. From this we conclude that the height of the water layer is smaller than the single-layer graphene height, which

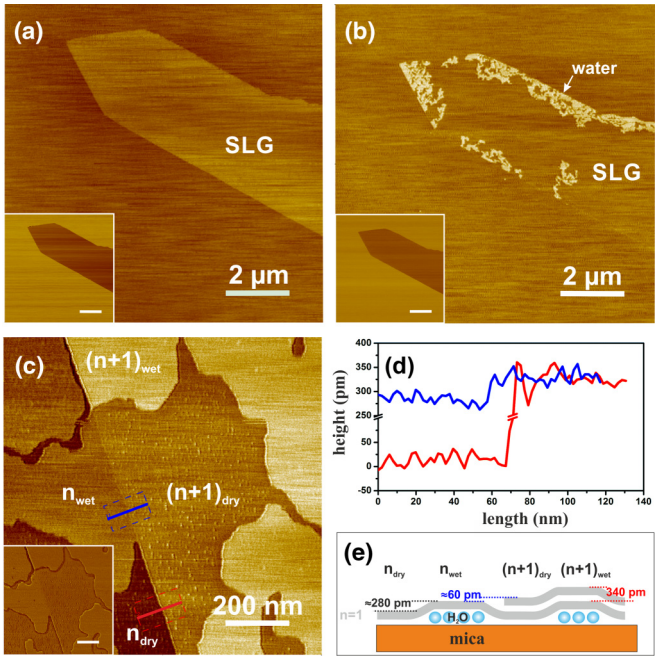

FIG. 1. SFM height images taken on mica partially covered with SLG in (a) less than 10 ppm of water and (b) 16% RH. The insets show phase images taken simultaneously with the height images. The dark areas on the phase images are the SLG. (c) SFM height image of a few-layer graphene with a single-layer step height terrace. The slit pore is partially filled with water. Inset shows phase image taken simultaneously with the height one. The black to white scales of all height and phase images are 1 nm and 10°, respectively. (d) Cross sections averaged over the red and blue rectangles in (c) showing that the $(n+1)$ graphene terrace unfilled with water is higher than the neighboring n graphene terrace filled with water. This implies that the water layer thickness is smaller than the single-layer graphene step height as it is sketched in (e).

is typically assumed to be equal to the interlayer spacing of 3.4 Å in graphite [Figs. 1(c)–1(e)] [23].

In the Raman studies, we first acquired Raman spectra on single-layer graphenes, which were exfoliated onto mica in a glove box with dry nitrogen (water <10 ppm). Then the samples were exposed to humidified nitrogen (50% RH), and Raman spectra were acquired again on essentially the same area as for the measurements in dry nitrogen. Comparison of Raman spectra acquired in dry and humid nitrogen [Figs. 2(a) and 2(b)] revealed a number of changes in G, $2D$, D, and D' peaks [20], which we report in the following. The data were acquired on two mica samples with 14 SLGs. At least two spectra were recorded for each SLG piece from spots separated by at least 3 μm. In attempts to (re-)activate the D' peak upon changing the humidity, we measured another four SLG pieces (see Sec. IV below).

The areas of the G peak did not vary significantly, neither between different SLGs (standard deviation 8% of the mean value) nor upon sample humidification. These minor changes can be attributed to drifts of the focal plane resulting in a small variation of collection efficiency and to differences in the mica thickness. The areas of other peaks are typically normalized to the area of the G peak in order to compare different experiments [24,25]. The $2D$ peak areas reproducibly increased from dry to wet [Fig. 2(c)]: $\langle I_{2D}/I_G\rangle$ changed from 2.4 ± 0.2 (dry) to 4.3 ± 0.2 (wet).

Raman spectra acquired on dry SLGs show a small peak centered at $1621 \pm 2(\pm 1.2\text{error})\,\text{cm}^{-1}$. The peak position implies it to be the D' peak, and we will hereafter refer to it correspondingly [26]. The D' peaks practically disappeared after samples were exposed to humidified nitrogen [Figs. 2(b) and 2(d)]: normalized peak areas $\langle I_{D'}/I_G\rangle$ changed from $1.3 \pm 0.44 \times 10^{-2}$ (dry) to $0.2 \pm 0.14 \times 10^{-2}$ (wet) and peak heights normalized to $2D\langle H_{D'}/H_{2D}\rangle$ changed from $2.9 \pm 0.6 \times 10^{-2}$ (dry) to $0.4 \pm 0.3 \times 10^{-2}$ (wet). For the four SLG pieces used to test a D' reactivation prediction (see Sec. IV), the $\langle I_{D'}/I_G\rangle$ changed from $1.3 \pm 0.35 \times 10^{-2}$ (dry) to $0.07 \pm 0.05 \times 10^{-2}$ (wet), and then to $1.0 \pm 0.2 \times 10^{-2}$ and $0.06 \pm 0.03 \times 10^{-2}$ upon subsequent drying and rehumidifying, respectively. Changes in the D peak were slightly less reproducible: for 3 out of 14 graphenes the D to G peak area ratios ($\langle I_D/I_G\rangle$) decreased from $8 \pm 4 \times 10^{-2}$ (dry) to $3 \pm 1.5 \times 10^{-2}$ (wet), while for the other 11 graphenes it remained constant within the error.

Both G and $2D$ peak positions acquired on SLGs shifted upon increasing the humidity. The shift of the peaks is typically attributed to doping or strain in graphene or a combination thereof. Since it has been argued that the $2D$ vs G peak position dependence can be used to differentiate between doping and strain [27], we plot the 2D vs G peak positions [Fig. 3(a)]. While the $2D$ and G peak positions scatter substantially for dry samples, the scattered data can be fitted well with a line of slope 2.2 ± 0.1, where the error is the standard error (SE). Exposure to humid nitrogen shifted the $2D$ and G peak positions to a more limited area in the $2D$ vs G graph. The widths of the $2D$ and G peaks also changed from dry to wet [Fig. 3(b)]: The G peak width increased from $9.1 \pm 1.2\,\text{cm}^{-1}$ to $14.1 \pm 1.5\,\text{cm}^{-1}$, while the $2D$ peak width decreased from $31.2 \pm 2.4\,\text{cm}^{-1}$ to $23.8 \pm 1.1\,\text{cm}^{-1}$. To gain more insight into $2D$ and G peak width changes from dry to wet, we plotted $2D$ vs G peak widths [Fig. 3(b)]. The widths of $2D$ and G peaks for dry samples scatter and linear fitting gives a slope of 1.7 ± 0.2 with the error here being SE.

IV. DISCUSSION

We will discuss first the SFM images. Contrasts in phase images are known to reveal the differences in tip-sample interactions and thus can be interpreted as material contrasts [32,33]. Thus phase images [Fig. 1(a)–1(c)] imply water islands to be confined between graphene and mica and not reside on top of graphene. Furthermore, graphene is known to be impermeable to small molecules [34,35]. Therefore, we attribute the flat islands growing upon increase of humidity to a layer of water molecules moving into the slit pore from its edges. The height of the islands implies the layer to be monomolecularly thick [36]. The expected height of an I_h ice bilayer is 3.7 Å [3], significantly higher than what we observed (less than 3.4 Å), which supports our conclusion of a monomolecular thickness of the layer. Still, the SFM data alone do not allow one to exclude a possibly thicker than a monolayer film of water molecules confined in the slit pore at high humidities, even though we observe only a monolayer,

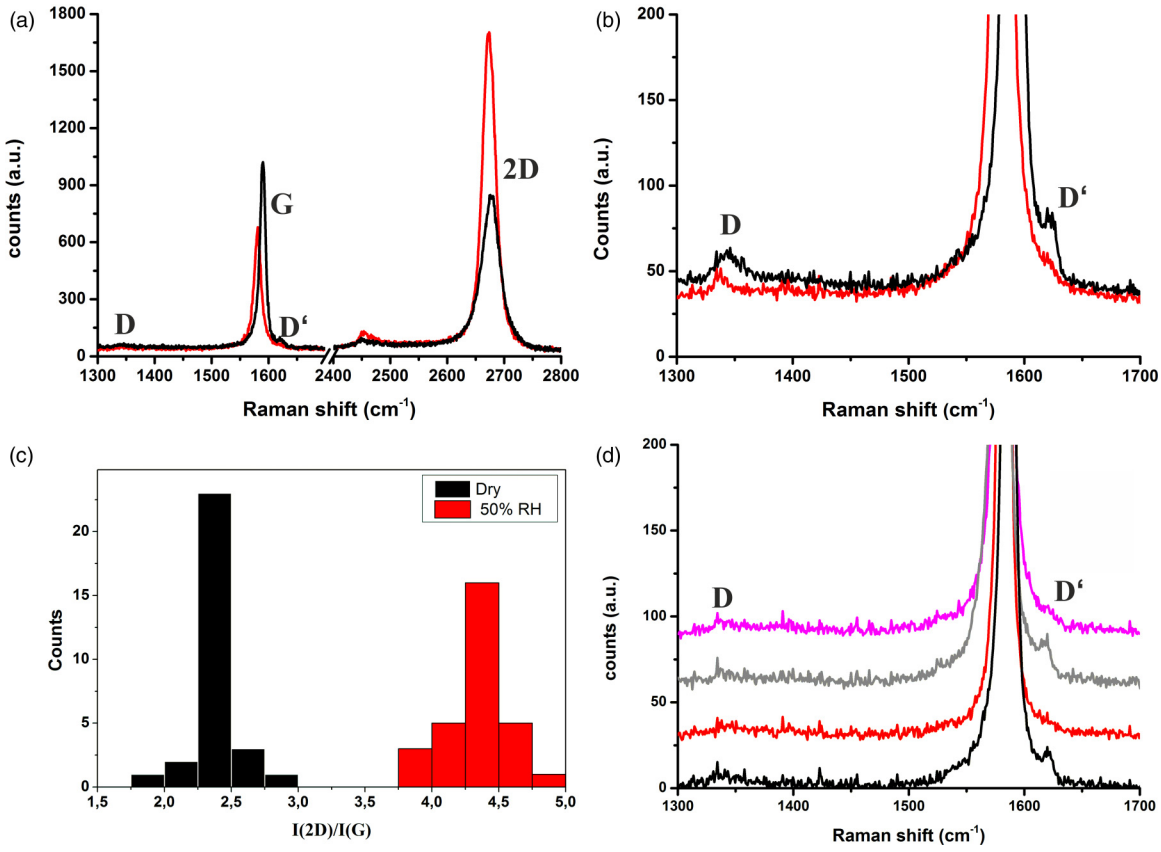

FIG. 2. (a) Raman spectra acquired on a single-layer graphene in dry (black line) and humidified (RH 50%, red line) nitrogen environments. The G, $2D$, D, and D' peaks are labeled. (b) Magnified D and D' spectral and intensity ranges. (c) Histograms of peak area ratios for $2D$ to G for dry (black) and humidified (red) SLGs. (d) Raman spectra acquired on a single-layer graphene used to test a D' reactivation prediction (see Sec. IV) in dry (black line), humidified (RH 50%, red line), dried again (RH 2.5%, gray line), and rehumidified (RH 50%, magenta line) nitrogen environments. The spectra are offset along the Y axis for clarity.

which wets and dewets the pore: We cannot exclude that the mica surface had been covered with a layer of water molecules before exfoliation of graphenes, i.e., graphenes reside on a layer of water under "dry" conditions. Indeed, assuming a sticking coefficient of 1 for water molecules impinging the surface of mica in the glove box, the mica surface should become covered with a monolayer of water within less than a second under 5 ppm water content [37]. We will argue in the following that the Raman data imply that it is not the case, i.e., graphenes lie directly on the mica surface when exfoliated under dry nitrogen.

The presence of structural defects in graphene activates both D and D' peaks around 1350 and 1621 cm^{-1}, respectively, with the intensity of the D peak being comparable and typically even exceeding the D' peak intensity [26,38]. The ratio of D to D' is known to be sensitive to the type of defect. The reduction of the D' peak intensity while the D peak remains unchanged implies that the reason for the D' peak in our case is not structural defects in graphene. It has been predicted that charge impurities located in close proximity to the graphene plane should selectively activate the D' peak [39]. The calculations were performed for $10^{12}\ \mathrm{e}^-/\mathrm{cm}^2$ charge impurity density and it was argued that the D' peak intensity was quite low: the ratio of D' to $2D$ peak height was calculated to be $\langle H_{D'}/H_{2D}\rangle = 1.7 \times 10^{-4}$ (as extracted from Ref. [39], Fig. 18). Muscovite mica consists of aluminosilicate layers with a negative surface charge, kept together by interlayers of potassium cations (K^+). Cleavage of mica propagates along the K^+ layers with presumably about half of the K^+ remaining on either surface; the exact distribution of the ions is unknown [6]. The surface of muscovite mica has a hexagonal unit cell with the cell side of 5.2 Å and one K^+ per unit cell. Thus, cleavage should result in a K^+ surface density of about $2 \times 10^{14}\ \mathrm{cm}^{-2}$, i.e., 200 times larger than the value assumed for the calculations. We remind that in our case the $\langle H_{D'}/H_{2D}\rangle$ for dry graphenes was $2.9 \pm 0.6 \times 10^{-2}$. Thus we assign the small peak we find around 1621 cm^{-1} to the D' peak activated by a direct contact with the K^+ layer, and the disappearance of the peak at high humidities to a water monolayer, which decouples graphene from mica.

It has been shown that reduction of humidity causes partial dewetting of the water monolayer [5]. This implies that drying should cause partial reactivation of the D' peak. We tested this prediction on a few SLGs, and the data support the prediction. Thus, presence of the D' peak for dry samples implies no water between mica and graphene. We will discuss in the following further evidence supporting this conclusion.

Strain in graphene and charge-doping both are expected to shift G and $2D$ peak positions albeit with very different ratios of $\Delta\omega_{2D}/\Delta\omega_G$. Therefore, it has been proposed to plot

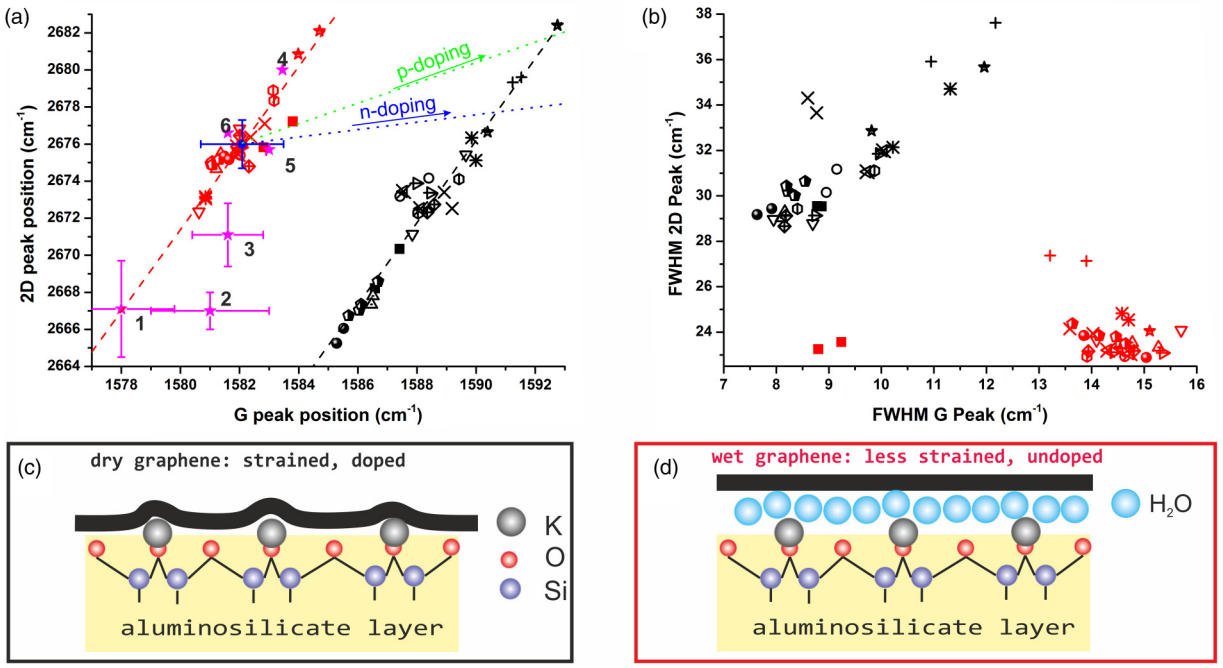

FIG. 3. (a) $2D$ versus G peak positions and (b) FWHMs for dry (black symbols) and humidified (red symbols) SLGs. Different symbols show results from different graphene pieces. The pink stars in (a) labeled with **1–6** are the literature values for undoped and possibly unstrained graphenes: **1** [28], **2** [29], **3** [27], **4** [30], **5** [21], and **6** [31] (see Sec. IV for the details). The blue square in (a) shows the averaged $2D/G$ peak position for the humidified SLGs; the error bars show the sum of SEs and the instrumental error. Green and blue dotted lines have slopes of 0.55 and 0.2 and show the expected shifts of $2D$ and G peak positions for p- and n-doping, respectively [31]. The dashed lines in (a) have a slope of 2.2 and are guides for the eye. The results for dry samples can be explained with combination of either p- or n-doping and mostly tensile strain. (c) Cleavage of mica presumably removes half of potassium ions. We suggest that graphenes become strained when exfoliated onto such surface. (d) A monolayer of water molecules filling into the slit pore between graphene and mica, possibly fills also the gaps between the K^+ ions removing thereby tensile strain in graphene.

$2D$ vs G peak positions to differentiate between influences of strain and charge-doping [27]. Tensile or compressive strains are expected to, respectively, downshift or upshift linearly the G and $2D$ peaks on the $2D$ vs G graph with the slope of about 2.2 [27]. p- and n-dopings are expected to upshift the G and $2D$ peaks also roughly linearly with the slopes of 0.55 and 0.2, respectively, for low doping levels as in our samples [31]. The influences of strain and charge-doping on G and $2D$ peak positions are additive. That is, expected $2D$ and G peak positions for strained and doped graphene can be found as a sum of the shifts expected for strain and doping [27]. Thus, further quantitative discussion of our data will require the reference values of the peak positions for an undoped and unstrained graphene. We included therefore a few literature values (**1–6**) for undoped and possibly unstrained graphenes into the $2D$ vs G peak positions graph [Fig. 3(a)]. The $2D$ peak positions of the literature values have been recalculated to our excitation wavelength assuming their linear dependence on the excitation wavelength with the prefactor $74\,\mathrm{cm}^{-1}/\mathrm{eV}$ [40]. Point **1** was taken from Ref. [28] (sample C, as it has the smallest error). The error bars of **1** include also maximum possible strain following discussion by the authors [41]. Point **2** is taken from Ref. [29]. Point **3** was taken from Ref. [27] (suspended graphene sample); the error bars are the sum of the instrumental error and error on the peak positions. Point **4** was extracted from Ref. [30] (Fig. 3). Point **5** was extracted from Ref. [21] [Fig. 3(a), with the smallest G and $2D$ peak position values for samples M09 and M08 being least doped]. Point **6** was extracted from Ref. [31] (Figs. 4 and 6). Charge-doping in (**1–6**) has been either controlled to be zero, or the samples were argued to be sufficiently clean to be undoped. The strain has not been directly discussed in (**3–6**); the SLG samples were prepared by mechanical exfoliation and thus the samples could be randomly strained. Anisotropic strain in **1** has been argued to be less than 0.1%; isotropic strain has been argued to be improbable due to sample geometry.

The literature values (**1–3**) and (**4–6**) are for graphenes suspended and supported by dielectric substrates, respectively. It has been argued that screening by a dielectric substrate reduces the electron-phonon coupling at the high-symmetry point K which results in an upshift of the $2D$ peak [42]. This might explain the apparent difference between suspended (**1–3**) and substrate supported (**4–6**) graphenes [Fig. 3(a)]. Furthermore, we notice that average $2D$ and G peak positions from humidified samples match previously reported ones for graphene separated from mica by a layer of water molecules [point **5** in Fig. 3(a)] and argued to be undoped and unstrained [21]. Therefore, we assume in the following that averaging of $2D$ and G peak positions from humidified samples provides us the reference point of unstrained and undoped graphene: $\omega_G = 1582 \pm 1.4\,\mathrm{cm}^{-1}$ and $\omega_{2D} = 2676 \pm 1.3\,\mathrm{cm}^{-1}$ [blue square in Fig. 3(a); the errors are the sum of SEs and instrumental error]. The assumption of our graphenes in humidified samples to be undoped is supported by the large $2D/G$ peak area ratios

expected for charge-undoped graphene [43]. Furthermore, the conclusion is supported by the large G peak width from humidified samples matching the expected value for an undoped graphene. One out of 14 humidified SLGs was probably slightly doped for reasons unclear to us. Since the G peak width for this piece was 9 cm^{-1}, the G peak position was slightly upshifted to 1583 cm^{-1} and the $2D/G$ peak area ratio was 3.9, i.e., smallest among all SLGs (Figs. 2 and 3).

We attribute the scattering of $2D$ and G peak positions from dry samples along the line with slope of 2.2 to different strains in the SLGs [Fig. 3(a)]. Then, the dry SLGs must be uniformly doped. Our data do not allow us to discuss whether it is p- or n-doping. It has been argued previously that SLGs lying directly on mica became p-doped by the substrate with $\Delta\omega_G \sim 12$ cm^{-1} offset of the G peak between undoped and mica-doped SLGs [21]. Assuming p-doping also in our case implies $\Delta\omega_G \sim 10$ cm^{-1} between dry and humidified samples [Fig. 3(a)], in good agreement with the previous investigation. The difference in doping between dry and humidified samples has been explained with the water layer gating the charge transfer between graphene and mica [21]. This further supports our conclusion on SLGs being in direct contact with mica in dry samples.

The data for the dry samples can be explained with the combination of a certain p-doping and variable tensile strains. It is tempting to attribute tensile strain in dry graphene samples to graphene deformation on the underlying K^+ layer [Fig. 3(c)]. The average distance between K^+ ions should be 0.7 nm assuming that only half of the ions remain on the surface after cleavage. Resolution of the SFM in tapping mode is not high enough to resolve this. We will discuss below that our data provide further support for dry SLGs being locally strained on the K^+ layer. Both $2D$ and G peak widths from our dry samples exceed the expected ones for charge-doped and unstrained graphenes [30]. The graph of the $2D$ peak widths plotted vs G ones for dry SLGs shows a clear correlation between $2D$ and G peak widths [Fig. 3(b)]. Furthermore, the widths of the peaks and peak positions appear to be quite reproducible within a given SLG piece, while they vary from piece to piece [Figs. 3(a) and 3(b)]. To support this observation we calculated total- and intrasample mean absolute deviations (MADs) of $2D$ peak positions (ω) and widths (Γ) for dry samples: $\mathrm{MADtotal/intra}(\omega_{2D}) = 3.3/0.8$ and $\mathrm{MADtotal/intra}(\Gamma_{2D}) = 1.9/0.5$, respectively. We note that for a purely random scattering of values one would expect the same values for the total- and intrasample MADs. The reproducible broadening of the peaks may be attributed to local strains in graphene, given by the misalignment between graphene and K+ lattices, similarly to the case of graphene on hexagonal boron nitride [44]. This should lead to inhomogeneous peak broadening with the slope of about 2.2 on the $2D$ peak width vs G peak width graph [27,45,46]. The slope is slightly smaller in our case. This could be the result of electric charge redistribution in graphene due to the close proximity to the ionic mica surface. The inhomogeneous charge distribution in graphene should result in peak broadening with the slope of 0.55 on the $2D$ width vs G peak width graph for the assumed p-doping. That is, inhomogeneous doping should result in substantial G peak broadening which is not accompanied by a strong $2D$ peak broadening and can shift the quotient of peak widths to lower values. The lack of information on K^+ distribution prevents us from further discussion on the possible influence of inhomogeneities of strain and charge distributions on peak broadening. The detailed analyses of peak broadening may be done in subsequent work.

Cleavage of the mica removes half of the K^+ ions, leaving gaps between the ions. The size of the K^+ ions roughly matches the size of the water molecules [47]. Thus, one can expect water molecules to fill the gaps between the ions, effectively flattening the surface and thus removing the tensile strain in graphene [Figs. 3(c) and 3(d)]. Remaining random strains could be inherited from mechanical exfoliation and persist from dry to humidified samples. The flat islands with the height of 2.8 Å seen by SFM should be a monolayer of water molecules growing on top of the first mixed layer of ions and water molecules [Fig. 3(d)]. Possibly, however, the bilayer model is an oversimplification and understanding of the film properties does not allow one to treat the two layers independently. This might be especially true in case some of the potassium ions are replaced with other types of ions with different ionic radii.

V. CONCLUSIONS

SFM and Raman data show that graphene is charge-doped and strained when exfoliated onto mica and measured under dry nitrogen. Upon increasing the nitrogen humidity to about 50% a monolayer of water wets the graphene-mica slit pore, removing doping and reducing strain in graphene. Furthermore, the D' peak practically disappears upon wetting, and recurs when the water layer dewets the pore. We attribute the D' peak to a direct contact of the graphene with the ionic mica surface, and we conclude from this that graphene is in direct contact with mica in dry samples, while a monolayer of water wetting the slit pore decouples the graphene from the mica substrate both mechanically and electronically. The mica surface consists of a layer of potassium ions, which may possibly mix with the water molecules wetting the slit pore. The structure of the mixed layer is not fixed by covalent bonds and can thus reshape. This may have to be accounted for in order to better understand the layer properties.

More generally, we demonstrated that Raman spectroscopy allows to unravel strain and charge-doping in graphene upon wetting and dewetting of a graphene-mica slit pore with a monolayer of water. This makes the graphene-mica slit pore an attractive experimental system for better understanding of strain and charge-transfer influences on the sorption of liquids by porous materials and transport of liquids in nanoconfinements.

[1] R. R. Nair, H. A. Wu, P. N. Jayaram, I. V. Grigorieva, and A. K. Geim, Science **335**, 442 (2012).

[2] R. K. Joshi, P. Carbone, F. C. Wang, V. G. Kravets, Y. Su, I. V. Grigorieva, H. A. Wu, A. K. Geim, and R. R. Nair, Science **343**, 752 (2014).

[3] K. Xu, P. G. Cao, and J. R. Heath, Science **329**, 1188 (2010).
[4] N. Severin, M. Dorn, A. Kalachev, and J. P. Rabe, Nano Lett. **11**, 2436 (2011).
[5] N. Severin, P. Lange, I. M. Sokolov, and J. P. Rabe, Nano Lett. **12**, 774 (2012).
[6] H. K. Christenson and N. H. Thomson, Surf. Sci. Rep. **71**, 367 (2016).
[7] Y. X. Zhu and S. Granick, Phys. Rev. Lett. **87**, 096104 (2001).
[8] S. H. Khan, G. Matei, S. Patil, and P. M. Hoffmann, Phys. Rev. Lett. **105**, 106101 (2010).
[9] U. Raviv, P. Laurat, and J. Klein, Nature (London) **413**, 51 (2001).
[10] N. Severin, J. Gienger, V. Scenev, P. Lange, I. M. Sokolov, and J. P. Rabe, Nano Lett. **15**, 1171 (2015).
[11] N. Severin, I. M. Sokolov, and J. P. Rabe, Langmuir **30**, 3455 (2014).
[12] Q. Li, J. Song, F. Besenbacher, and M. D. Dong, Acc. Chem. Res. **48**, 119 (2015).
[13] P. Bampoulis, J. P. Witteveen, E. S. Kooij, D. Lohse, B. Poelsema, and H. J. W. Zandvliet, ACS Nano **10**, 6762 (2016).
[14] J. Gienger, N. Severin, J. P. Rabe, and I. M. Sokolov, Phys. Rev. E **93**, 043306 (2016).
[15] B. Rezania, M. Dorn, N. Severin, and J. P. Rabe, J. Colloid Interface Sci. **407**, 500 (2013).
[16] P. Bampoulis, D. Lohse, H. J. W. Zandvliet, and B. Poelsema, Appl. Phys. Lett. **108**, 011601 (2016).
[17] J. Song, Q. Li, X. F. Wang, J. Y. Li, S. Zhang, J. Kjems, F. Besenbacher, and M. D. Dong, Nat. Commun. **5**, 4837 (2014).
[18] C. Thomsen and S. Reich, Phys. Rev. Lett. **85**, 5214 (2000).
[19] A. C. Ferrari, Solid State Commun. **143**, 47 (2007).
[20] A. C. Ferrari and D. M. Basko, Nat. Nanotechnol. **8**, 235 (2013).
[21] J. Shim, C. H. Lui, T. Y. Ko, Y. J. Yu, P. Kim, T. F. Heinz, and S. Ryu, Nano Lett. **12**, 648 (2012).
[22] M. Dorn, P. Lange, A. Chekushin, N. Severin, and J. P. Rabe, J. Appl. Phys. **108**, 106101 (2010).
[23] J. D. Bernal, Proc. R. Soc. London, Ser. A **106**, 749 (1924).
[24] D. M. Basko, S. Piscanec, and A. C. Ferrari, Phys. Rev. B **80**, 165413 (2009).
[25] Z. H. Ni, T. Yu, Z. Q. Luo, Y. Y. Wang, L. Liu, C. P. Wong, J. M. Miao, W. Huang, and Z. X. Shen, ACS Nano **3**, 569 (2009).
[26] R. Beams, L. G. Cancado, and L. Novotny, J. Phys.: Condens. Matter **27**, 083002 (2015).
[27] J. E. Lee, G. Ahn, J. Shim, Y. S. Lee, and S. Ryu, Nat. Commun. **3**, 1024 (2012).
[28] S. Berciaud, S. Ryu, L. E. Brus, and T. F. Heinz, Nano Lett. **9**, 346 (2009).
[29] D. Metten, F. Federspiel, M. Romeo, and S. Berciaud, Phys. Status Solidi B **250**, 2681 (2013).
[30] A. Das, S. Pisana, B. Chakraborty, S. Piscanec, S. K. Saha, U. V. Waghmare, K. S. Novoselov, H. R. Krishnamurthy, A. K. Geim, A. C. Ferrari, and A. K. Sood, Nat. Nanotechnol. **3**, 210 (2008).
[31] G. Froehlicher and S. Berciaud, Phys. Rev. B **91**, 205413 (2015).
[32] I. Schmitz, M. Schreiner, G. Friedbacher, and M. Grasserbauer, Appl. Surf. Sci. **115**, 190 (1997).
[33] J. P. Cleveland, B. Anczykowski, A. E. Schmid, and V. B. Elings, Appl. Phys. Lett. **72**, 2613 (1998).
[34] J. S. Bunch, S. S. Verbridge, J. S. Alden, A. M. van der Zande, J. M. Parpia, H. G. Craighead, and P. L. McEuen, Nano Lett. **8**, 2458 (2008).
[35] P. Lange, M. Dorn, N. Severin, D. A. Vanden Bout, and J. P. Rabe, J. Phys. Chem. C **115**, 23057 (2011).
[36] G. Algara-Siller, O. Lehtinen, F. C. Wang, R. R. Nair, U. Kaiser, H. A. Wu, A. K. Geim, and I. V. Grigorieva, Nature (London) **519**, 443 (2015).
[37] G. Burns, *Solid State Physics* (Academic, New York, 1985).
[38] A. Eckmann, A. Felten, I. Verzhbitskiy, R. Davey, and C. Casiraghi, Phys. Rev. B **88**, 035426 (2013).
[39] P. Venezuela, M. Lazzeri, and F. Mauri, Phys. Rev. B **84**, 035433 (2011).
[40] R. Narula and S. Reich, Phys. Rev. B **78**, 165422 (2008).
[41] M. Y. Huang, H. G. Yan, C. Y. Chen, D. H. Song, T. F. Heinz, and J. Hone, Proc. Natl. Acad. Sci. USA **106**, 7304 (2009).
[42] F. Forster, A. Molina-Sanchez, S. Engels, A. Epping, K. Watanabe, T. Taniguchi, L. Wirtz, and C. Stampfer, Phys. Rev. B **88**, 085419 (2013).
[43] D. Metten, G. Froehlicher, and S. Berciaud, Phys. Status Solidi B **252**, 2390 (2015).
[44] A. Eckmann, J. Park, H. Yang, D. Elias, A. S. Mayorov, G. Yu, R. Jalil, K. S. Novoselov, R. V. Gorbachev, M. Lazzeri, A. K. Geim, and C. Casiraghi, Nano Lett. **13**, 5242 (2013).
[45] C. Neumann, S. Reichardt, P. Venezuela, M. Drögeler, L. Banszerus, M. Schmitz, K. Watanabe, T. Taniguchi, F. Mauri, B. Beschoten, S. V. Rotkin, and C. Stampfer, Nat. Commun. **6**, 8429 (2015).
[46] D. Metten, F. Federspiel, M. Romeo, and S. Berciaud, Phys. Rev. Appl. **2**, 054008 (2014).
[47] R. D. Shannon, Acta Cryst. A **32**, 751 (1976).